UDK 620.186:669.715
Original scientific article/Izvirni znanstveni članek

ISSN 1580-2949
MTAEC9, 57(6)663(2023)

INFLUENCE OF NICKEL ON THE MICROSTRUCTURAL EVOLUTION AND MECHANICAL PROPERTIES OF LM6-ALLOY-BASED FUNCTIONALLY GRADED COMPOSITE TUBES

VPLIV VSEBNOSTI NIKLJA NA MIKROSTRUKTURO IN RAZVOJ MEHANSKIH LASTNOSTI KOMPOZITNIH FUNKCIONALNO GRADUIRANIH CEVI NA OSNOVI ZLITINE VRSTE LM6

A. Saiyathibrahim[1], S. Santhosh[2], G. Raja Kumar[3], S. Bharani Kumar[4]

[1]Department of Mechanical Engineering, Karpagam Institute of Technology, Coimbatore, Tamil Nadu 641 105, India
[2]Department of Mechanical Engineering, Sri Krishna College of Technology, Coimbatore, Tamil Nadu 641 042, India
[3]Department of Mechanical Engineering, Swarna Bharati Institute of Science and Technology, Khammam, Telangana 507 002, India
[4]Department of Mechanical Engineering, Rajalakshmi Institute of Technology, Kuthambakkam, Tamil Nadu 600 124, India

Prejem rokopisa – received: 2023-02-20; sprejem za objavo – accepted for publication: 2023-10-22

doi:10.17222/mit.2023.799

Despite the growing demand for new materials, we used the horizontal centrifugal casting technique to synthesize functionally graded composite (FGC) tubes using an LM6 alloy containing (3, 6 and 9) *w*/% nickel. All the fabricated tubes were evaluated for variations in microstructure, hardness and tensile properties along the radial cross-section in three distinct zones (inner, transition and outer). X-Ray diffraction (XRD) results indicated the formation of *in-situ* Al_3Ni in all FGC tubes, and these *in-situ* tri-aluminides increased further with the addition of Ni. A comprehensive microstructural analysis across the tubes utilising scanning electron microscopy (SEM) images showed that gathering *in-situ* Al_3Ni particles keeps growing nearer the outer zone, and primary Si cuboids increase in the inner zone. This accumulation of particles improved the mechanical properties at all three zones of the FGC tubes compared to the LM6 tube having no nickel. The results of the hardness investigation showed that precipitated Al_3Ni in FGCs has a beneficial impact on the enhancement of hardness. Furthermore, the observed UTS improvement in the FGC tubes was clearly associated with the precipitation and strengthening action of Al_3Ni intermetallic phases, while a significant reduction in elongation has been noted. Due to the influence of centrifugal force and density variation, the tube containing 9 *w*/% of Ni demonstrated good gradation among composite alloy-fabricated FGC tubes, with *in-situ* Al_3Ni particles settling largely in the outer zone and primary Si particles settling primarily in the inner zone across the radial thickness.

Keywords: functionally graded composite, microstructure, hardness, tensile strength

Zaradi povpraševanja po novih inventivnih materialih so se avtorji posvetili razvoju proizvodnje funkcionalno graduiranih kompozitnih cevi (FGC; angl.: Functionally Graded Composite) s tehniko horizontalnega centrifugalnega litja. Za sintezo trislojne kompozitne cevi z različno strukturo in lastnostmi so kot osnovo uporabili Al zlitino vrste LM6 s (3, 6 in 9) *w*/% niklja (Ni). Vse izdelane kompozitne cevi so okarakterizirali glede na variranje mikrostrukture, trdote in mehanskih lastnosti vzdolž radialnega preseka posameznih treh slojev (notranje prehodne in zunanje cone oziroma plasti). Rezultati analiz z rentgensko difrakcijo (XRD; angl.: X-Ray Diffraction) kažejo na *in-situ* tvorbo Al_3Ni v vseh FGC ceveh in vsebnost teh *in-situ* nastalih tri-aluminidov narašča z naraščajočo vsebnostjo Ni. Obsežne mikrostrukturne preiskave z uporabo vrstične elektronske mikroskopije (SEM; angl.: Scanning Electron Microscopy) preko cevi so pokazale, da se *in-situ* nastali Al_3Ni delci zbirajo in rastejo v bližini zunanje cone cevi, medtem ko se primarne Si kockice nahajajo znotraj notranje plasti cevi. To zbiranje oziroma kopičenje delcev izboljša mehanske lastnosti vseh treh slojev FGC v primerjavi s cevjo iz osnovne Al zlitine brez dodatka Ni. Meritve trdote so pokazale, da izločeni delci Al_3Ni v FGCs ugodno vplivajo na povišanje trdote. Nadalje so natezni preizkusi izvedeni na preizkušancih iz posameznih slojev cevi jasno pokazali izboljšanje končne natezne trdnosti (UTS; angl.: ultimate tensile strength) zaradi izločanja in utrjevalnega učinka intermetalne faze Al_3Ni. Istočasno so opazili pomembno zmanjšanje raztezka zlitin. Zaradi vpliva centrifugalne sile in variranja gostote ima cev z vsebnostjo 9 *w*/% Ni najboljšo lastno gradacijo med vsemi izdelanimi kompozitnimi zlitinami FGC cevi z *in-situ* nastalimi Al_3Ni delci, ki se večinsko nahajajo v zunanji plasti kompozitne cevi in primarni Si delci, ki se večinsko nahajajo v notranjem sloju notranje plasti vzdolž radialne debeline cevi.

Ključne besede: funkcionalno graduirani kompoziti, mikrostrukture, trdota, natezna trdnost

1 INTRODUCTION

Functionally Graded Composites (FGCs) are sophisticated multifunctional structures that have recently sparked widespread interest. The distribution of reinforcements in all such FGCs varies linearly from one end to the other in the constructed component.[1] This gradient composition makes these materials preferable in many applications, such as cylinder liners, brake rotor discs, pulleys, optical devices, armors, etc. Moreover, tailoring properties at specific locations in a matrix phase by introducing one or more reinforcements is more attractive for FGCs, which is impossible in conventional composites.[2,3] Among the various FGCs investigated recently, aluminium-based FGCs have been reported as having better mechanical and tribological properties due to the inclusion of reinforcements in appropriate volume proportions. Nowadays, aluminides such as Al_3Ti, Al_2Cu, AlB_2, Al_3Ni, and Al_3Zr are used instead of ceramics to impart advantages like high thermal stability, elastic

*Corresponding author's e-mail:
imsaiyath@gmail.com (Saiyathibrahim A.)

modulus, hardness and low thermal expansion coefficient. These aluminides also provide a strong bond between reinforcements and matrix, lowering the residual stresses. Hence, the degree of failure is reduced during the thermal loading cycle of components.[4]

Aluminium-silicon (Al-Si) alloys are widely utilised as engineering materials to manufacture castings, particularly in the automotive, military and aerospace sectors, attributed to their superior strength-to-weight ratio, strong thermal conductivity, great castability, simplicity of fabrication and lightweight. The LM6 alloy is one of several Al-Si alloys that are extensively used to make components such as cylinder blocks and pistons. However, the mechanical properties of this alloy have been observed to be reduced by microstructural flaws like dendrites and silicon morphology.[5–7] In general, alloying metals such as Cu, Ce, B, Ni and Mg encourage the formation of intermetallic compounds, altering the properties of Al-Si alloys. These alloying elements can influence the properties by way of precipitation hardening and solid-solution strengthening to create new low-density, high-durability components.[8] Nickel has a very low solid solubility in aluminium and therefore forms Al_3Ni intermetallic after the solubility limit is reached. Furthermore, Ni has been identified to be the most effective constituent for improving the high-temperature characteristics of Al-Si alloys. Golmohammadi et al.[9] proposed that adding Ni to LM6 alloy stimulated the development of Al_3Ni particles, which seemed to be related to expanded wear resistance and hardness. Yang et al.[10] reported that incorporating Ni into an Al-Si alloy boosted its ultimate tensile strength while decreasing its elongation. Research related to Al_3Ni tri-aluminide reported that this intermetallic has high hardness (841HV), which can be used for the production of *in-situ* composites.[11] These hard intermetallic phases are usually dispersed in a ductile matrix to overcome low ductility and fracture toughness, resulting in a good structural composite material.

Centrifugal casting is a simple process for producing cylindrical FGCs with great microstructural control and good mould filling, providing better properties. The continuous gradient in FGC using centrifugal casting is achieved by centrifugal force created during mould rotation. The change in density between the molten matrix and reinforcement particles encourages the formation of a gradient microstructure over the thickness of a cylindrical tube constructed with a matrix material that includes reinforcing particles (*in-situ* or *ex-situ*). During the centrifugal casting of an Al-Si alloy, it was revealed that due to the application of centrifugal force, primary Si particles migrated toward the inner surface across the radial thickness of the produced tube. The lower density of primary Si particles in comparison to the molten matrix has been identified as the origin of this reinforcement displacement and the production of non-uniform microstructures known as gradation.[12,13] Lin et al.[14] fabricated an Al-Si-Mg alloy tube in a centrifugal casting route, which possessed a particle-free outer zone and an inner zone with a lot of both *in-situ* Mg_2Si and primary Si reinforcements. The high proportion of these *in-situ* Mg_2Si particles was observed to increase the mechanical properties in Al-Mg_2Si FGCs, such as hardness and tensile strength in the inner zone.[15,16] Duque et al.[17] claimed that adding boron to aluminium increased the hardness in the outer zone by precipitating and segregating *in-situ* AlB_2 reinforcement in a centrifugally cast tube. Rajan et al.[18] achieved an outstanding gradient structure in an Al-Ni alloy-based FGC tube by constituting a high-density *in-situ* Al_3Ni-rich outer zone and an intermetallic free inner zone. Further, it was highlighted that in FGCs, centrifugal force is vital in creating gradation. The sorting of reinforcements over the radial thickness has been observed to be good at high centrifugal force, and particle settling at various zones is determined by their density. To be simpler, greater density reinforcements settle in the outside zone, and their concentration decreases as they approach the inner zone, whereas lighter particles do the opposite.[19]

Considering the existing literature, it can be asserted that certain aluminium alloy-based FGCs created by centrifugal casting and reinforced with several *in-situ* particles (Al_3Ti, Mg_2Si, Al_2Cu, AlB_2, Al_3Zr, Al_3Ni, etc) were methodically explored. However, there are many aluminium alloys to be investigated in this *in-situ* reinforcement context. The magnesium (Mg) effect on Al-Si alloys as well as the generation and dispersion of Mg_2Si particles along the radial cross-section of a centrifugally cast tube, has been extensively researched in the previous decade. However, there has been no reporting on the characteristics of graded composites created using an Al-Si alloy when introducing Ni, as well as the consequent morphological alterations and reinforcement settling processes. To bridge this gap, Ni was added to the LM6 alloy in different concentrations to form FGC tubes using a horizontal centrifugal casting in this study. Furthermore, the microstructural characteristics and mechanical properties have been studied across the thickness of the tubes. Also, the fracture mechanisms associated with the composites were discussed.

2 MATERIALS AND METHODS

The intended nickel concentrations of 3, 6 and 9wt% in the LM6 aluminium alloy were achieved by resistance melting of a commercially available LM6 alloy with Al-26%Ni master alloy in a graphite crucible. **Figure 1** shows the microstructural features examined using an optical microscope (OM) for an LM6 alloy with Al-26%Ni master alloy used to synthesize tubular specimens.

Table 1 shows the chemical composition of the alloys developed for this investigation as well as the designation of the manufactured tubes. To fabricate tubes, the prepared cast alloy bars were melted at a processing tem-

Table 1: Alloys used in the production of cast tubes and their chemical composition

Designation	Alloy used	Chemical composition in *w*/%							
		Si	Fe	Ni	Cu	Zn	Mn	Mg	Al
LM6 Tube	LM6 alloy	11.83	0.52	0.02	0.27	0.09	0.16	0.06	Balance
FGC_A Tube	LM6+3 *w*/%Ni	11.61	0.52	3.02	0.27	0.11	0.02	0.03	Balance
FGC_B Tube	LM6+6 *w*/%Ni	10.96	0.41	6.1	0.26	0.11	0.02	0.01	Balance
FGC_C Tube	LM6+9 *w*/%Ni	10.48	0.44	9.07	0.26	0.11	0.02	0.01	Balance

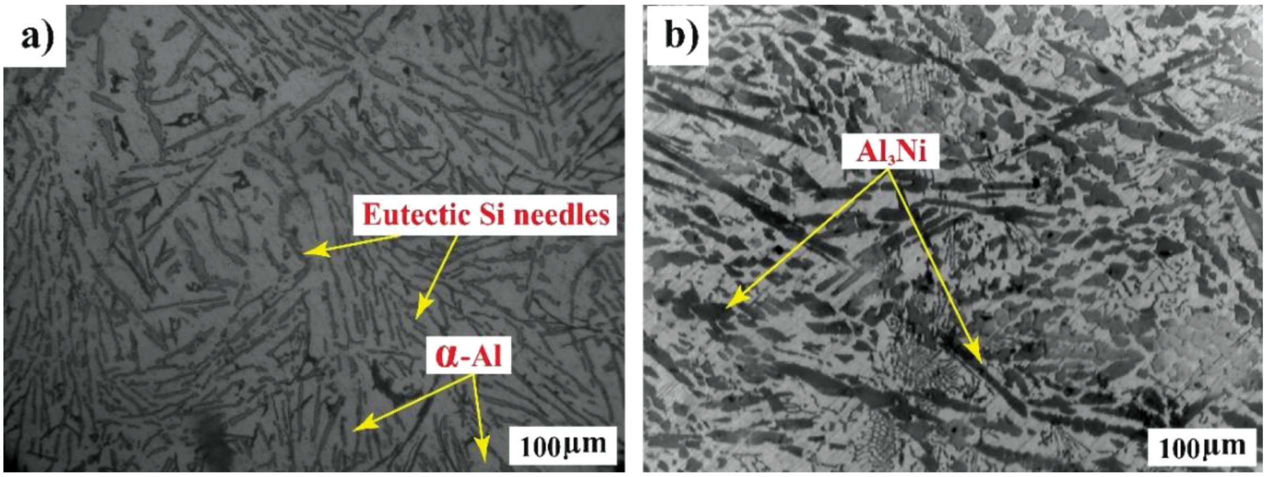

Figure 1: Microstructure of a) LM6 alloy b) Al-26%Ni master alloy

perature of 820°C under cover flux. A spinning graphite stirrer was used to mix the composite melt for 10 min after degassing (500 min^{-1}). The liquid metal was then poured into a cylindrical grey cast iron (GCI) mould (120 mm outer diameter & 110 mm length) that had been heated to 300 °C and was spinning at 1900 min^{-1} in a horizontal centrifugal casting machine.

A quantity of 950g melt was used to fabricate the tubular specimens (**Figure 2**) with an inner diameter of 50 mm, thickness of 15 mm, and length of 110 mm. Samples at three different zones (inner, middle, and outer) for quantitative and microstructural observations were prepared from the cast tubes, as shown in **Figure 2**. Microstructural examinations were carried out along the radial direction to observe zone-wise variations using scanning electron microscopy with energy-dispersive spectroscopy (SEM/EDS - JEOL JSM6360) following standard metallographic routines. As a further step, an image analyzer was used to evaluate the proportional volume of the reinforcement phase segregation.

Vickers hardness measurements were made at five spots (**Figure 2**) across the radial thickness in all tubes. The Vickers hardness (HV) is expressed as the indentation force/indentation area ratio, as seen in Equation (1).

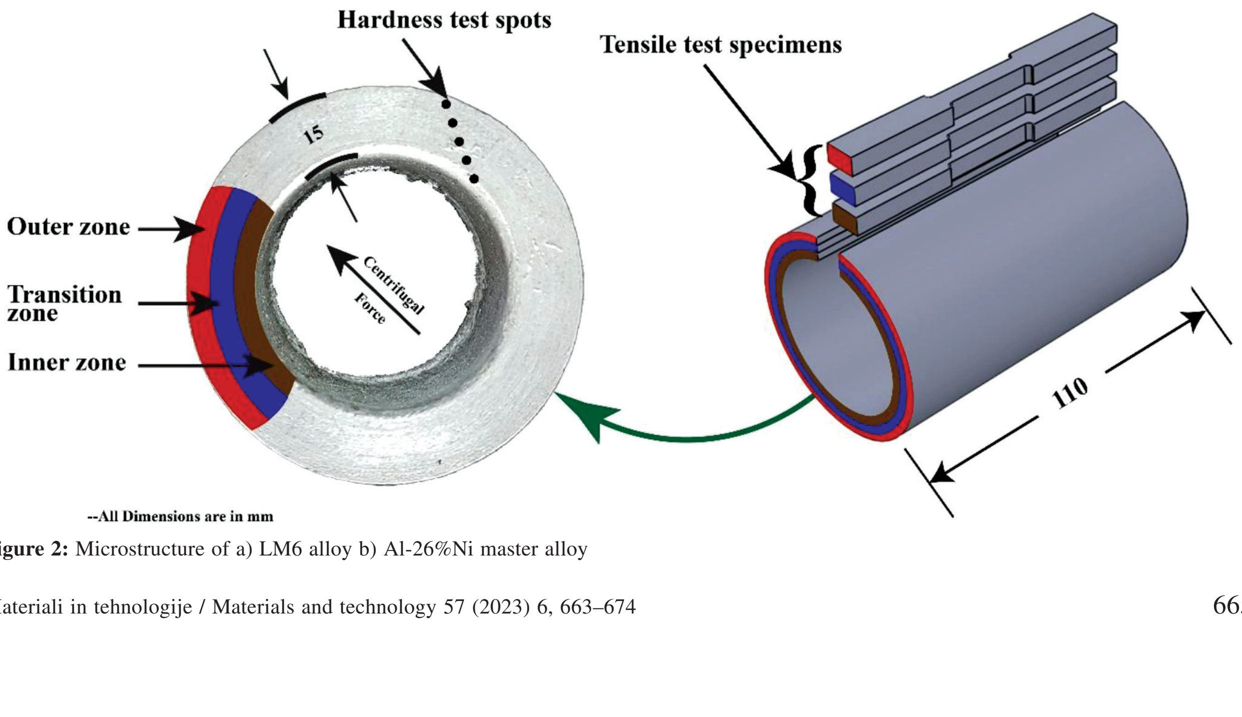

Figure 2: Microstructure of a) LM6 alloy b) Al-26%Ni master alloy

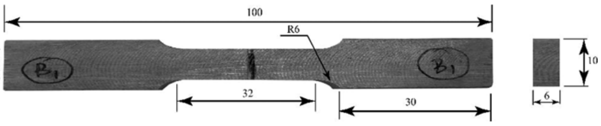

Figure 3: Dimensions of tensile test specimen

$$HV = \frac{2P\sin(\theta/2)}{d^2} \quad (1)$$

where P is the indentation load (in N), d is the indentation diagonal length (in mm) and θ is the indenter angle (in degrees).[20] The evaluations were conducted with a 50 g load and a 15 s dwell, and the values presented were the average of five repetitions. Tensile specimens were cut from three different zones by following ASTM: B-557M standard as shown in **Figure 3**. In order to find the crack path and fracture mode, fractured surfaces were examined by SEM.

3 RESULTS AND DISCUSSION

3.1 Microstructural Characterization

Cross-sections of the cylindrical tubes were taken in the radial direction and microstructures of both LM6 alloy and FGCs were accessed in three distinct zones: outer zone (within 5 mm), transition zone (5-10 mm), and inner zone (10-15 mm) as shown in **Figure 4**. The LM6 alloy tube microstructures (**Figure 4a** to **4c**)) consisted of a large quantity of flake-like eutectic Si phase embedded in the aluminium matrix with some cuboids of

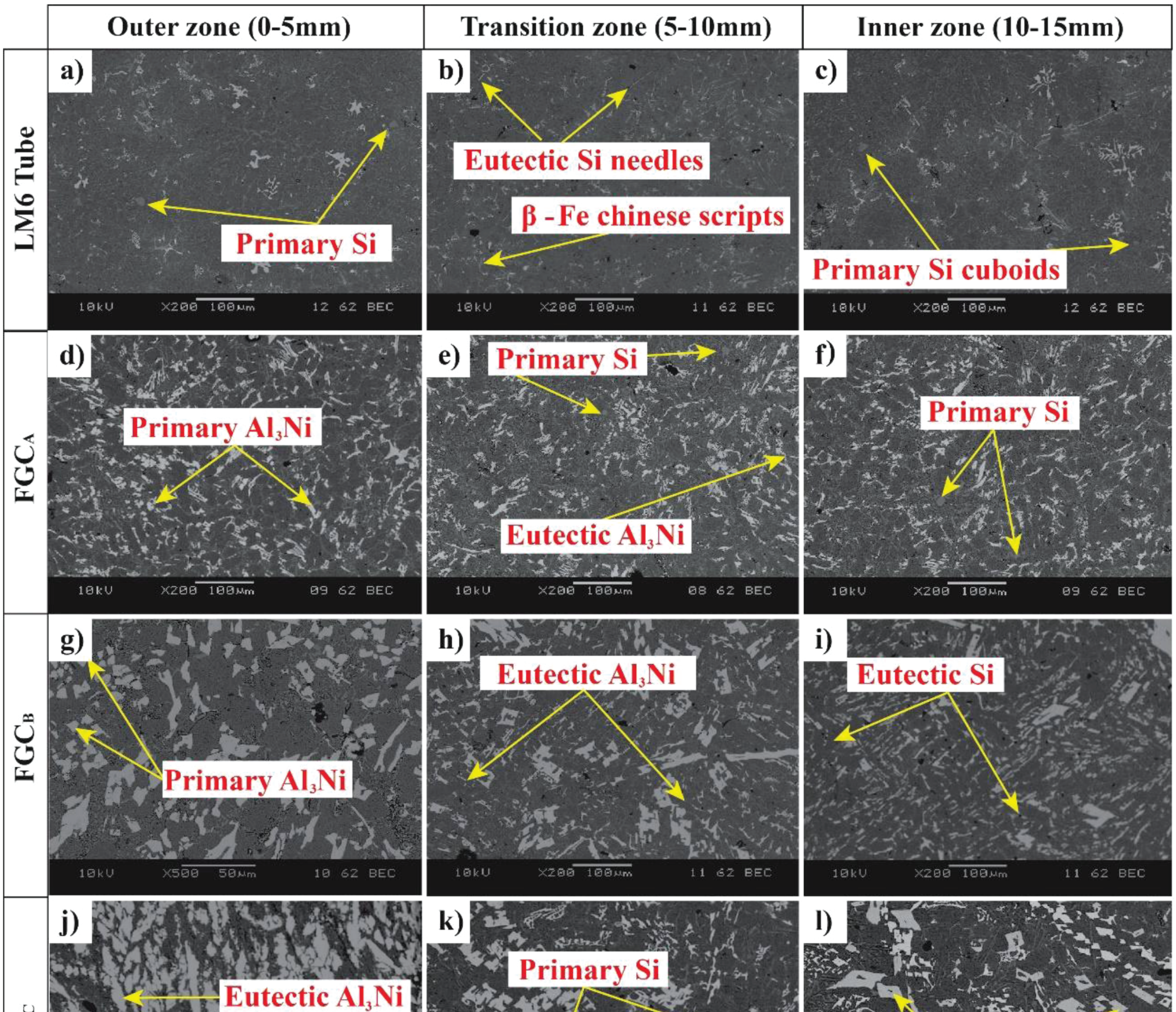

Figure 4: SEM images of LM6 tube and FGCs (FGC_A, FGC_B & FGC_C) at three different zones

primary Si. In general, the eutectic LM6 alloy contains eutectic Si phase and α-Al matrix.[21] Rapid cooling and directed solidification during the centrifugal casting process resulted in the nucleation of primary Si particles in the microstructure of the eutectic Al-Si alloy in its as-cast form.[22,23] Since solidification occurs in the above manner during centrifugal casting, it is conceivable for the LM6 alloy to include both eutectic Si phases and a substantial number of primary Si particles. Furthermore, it is frequently reported that increasing the silicon percentage in a cast Al-Si alloy increases the hardness by reducing the α-Al matrix.[24] Thus, it is reasonable to conclude that the Si phases are the key factor in increasing the hardness of the Al-Si alloy. Primary Si particle segregation in the LM6 tube was found to commence in the outer zone and reached its maximum in the inner zone. According to the microstructures, primary Si became less accessible in the direction of the centrifugal force. Besides, all three zones of the LM6 tube included eutectic Si flakes. Although there were some differences between the microstructures of the three zones considered for examination, they were not substantial enough to claim that a fine gradation is achieved in the LM6 tube. This minor gradation is because of the eutectic nature of the LM6 alloy and the presence of so few primary Si particles.

On the other hand, the microstructure of functionally graded composites (FGC_A, FGC_B & FGC_C) mainly consisted of the α-Al dendrite, primary silicon, eutectic silicon, primary Al_3Ni intermetallic and eutectic Al_3Ni intermetallic surrounded by their boundaries as illustrated in **Figure 4d–4l**). When compared to the LM6 tube sample, it was observed that the addition of Ni changes the eutectic silicon morphology to form primary Si cuboids.[23]

X-Ray diffraction (XRD) analysis of the LM6 tube showed the presence of two phases such as α-Al and Si; however, the FGC resulted in three phases such as Al_3Ni, Si, and α-Al, as seen in **Figure 5**. Considering that Ni and Si are only marginally soluble in the α-Al matrix (0.05 % and 0.1 % respectively), the generation of Al_3Ni

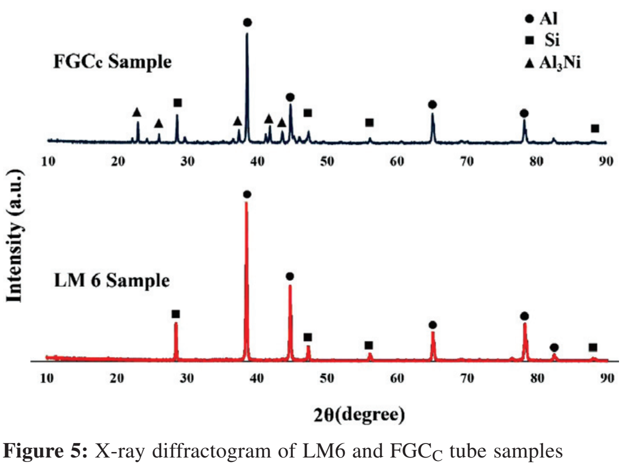

Figure 5: X-ray diffractogram of LM6 and FGC_C tube samples

tri-aluminide seems logical. It is important to note that intermetallic Al_3Ni has a very low solid solubility of Si, at only 0.5 %.[25] As a result, the interaction between the aluminium matrix and nickel was clearly the only way for an intermetallic compound to occur in the melt. It can also be said that the precipitation of the Al_3Ni phase depends on the quantity of nickel present in the composite melt. The stable Al_3Ni intermetallic phase was established in the melt through a ternary eutectic reaction between the nickel and the Al-Si alloy as mentioned in the following Equation (2):[26]

$$L \rightleftharpoons Al + Al_3Ni + Si \tag{2}$$

Centrifugal casting can be divided into two distinct subfields: centrifugal solid-particle method (CSPM) and centrifugal *in-situ* method (CISM) based on the target operating temperature.[27] The solid reinforcements, such as ceramic particles, are added externally into the melt in a CSPM. Also in these methods, the dispersed phase remains unchanged both chemically and physically throughout the process. In a centrifugal *in-situ* method, the reinforcements (intermetallics) are precipitating through chemical reactions inside the melt. The crystallisation phenomenon used here is very comparable to that used in *in-situ* composite manufacturing. The density difference between the primary crystals in the melt is responsible for the creation of compositional gradients during the CISM of fabricating FGCs.[12] These primary Al_3Ni particles and Si cuboids in melt under centrifugal force are amenable to the aforementioned formation mechanism. The primary Si particle has a density of 2.33 g/cm^3, whereas the Al_3Ni precipitate is reported to have a density of 4.0 g/cm^3.[18,28] These values are different from the molten aluminium (2.37 g/cm^3). Gradient distribution of the primary Al_3Ni and Si particles inside the FGC tubes was therefore anticipated.

The centripetal acceleration (a_p) and radial moving velocity (V_c) are responsible for the reinforcing particle segregation in different zones of the tube in centrifugal casting. They are expressed in Equations (3) and (4) as follows:

$$a_p = \frac{|\rho - \rho_l|}{\rho_p} 4\pi^2 N^2 r \tag{3}$$

$$V_c = \frac{d^2(\rho_p - \rho_l)\omega^2 r}{18\eta_c} \tag{4}$$

where N is the mould rotational velocity (s^{-1}), ρ_p is the reinforcement particle density, ρ_l is the density of composite melt (kg/m^3), r is the particle distance from the mould center (m), ω is the angular velocity of mould (rad/s), d is the diameter of the reinforcement particle (m) and η_c is the composite melt viscosity (Pa·s). Particles will migrate to the outer zone of the tube if $\rho_p > \rho_l$ and they will flow into the inner zone of the cast tube if $\rho_p < \rho_l$. The primary Si particles in the LM6 tube sample have a density (2.33 g/cm^3) that is less than the liquid metal (2.37 g/cm^3) and this density difference pushed the particles into the inner zone. Primary Al_3Ni particles in FGCs have a density of 4.0 g/cm^3 that is greater than that of the liquid metal, forcing the particles to the outer zone by centrifugal force.[18] At the same time, primary Si particles were being drawn inward (inner zone) by centripetal force in the case of the FGCs. This transportation occurred due to convection, which was increased by the considerable temperature difference formed during solidification between the outer and inner zones of the tube.[22,29]

From the microstructures of the FGC tubes (**Figure 4d–4l**)) it can be concluded that the gradation has been established in all three tubes. The formation of a gradient in the thickness of the FGCs was obtained by four phases. The primary Si cuboids in the melt were only partially retained in the outer zone of the tube at the beginning stage due to the cooling behaviour of the mould. As can be noticed in **Figure 4**, in the subsequent phase, numerous primary Si particles were pushed toward the inner zone by centripetal force. The third stage involved the segregation of the primary Al_3Ni particles that have precipitated within the melt. Intermetallic nucleation growth, development and transportation are all controlled by the temperature disparity established between the mould and poured liquid metal during solidification.[28] Due to their high density, primary Al_3Ni particles travelled to the outer zone, where they settled with the help of centrifugal force. The primary Si particles were likewise now heading towards a gradual inward migration at this stage. As the melt viscosity increases, primary Al_3Ni particles slow down and settle to a lower velocity in the final phase. Hence, both particles were not reaching their destinations as expected. They settled down quickly during the traveling time itself because of the rapid cooling nature of the centrifugal casting technique.

Figure 6 shows that the LM6 tube has primary Si cuboids traceable throughout the whole structure. The percentage of primary Si particles within the overall volume was calculated to be between 4.6 % and 6.0 %. Due to its eutectic composition, LM6 alloy had very few primary Si particles. The least volume fraction of primary Si (4.6 φ/%) was present in the outer zone; the inner and transition zones have far better segregation. These findings are in accordance with the respective microstructures of the LM6 tube (**Figure 4a–4c**).

As illustrated in **Figure 4**, it became evident that the primary Al_3Ni and Si particles had been segregated and accumulated in the inner and outer zones of all the FGCs with Ni levels of (3, 6 and 9) w/%. In FGC_A, the addition of 3 w/% of Ni promotes the formation of primary Al_3Ni particles to a value of 28 φ/% in the outer zone and primary Si particles to a value of 9.9 φ/% in the inner zone. The same trend has been observed in the other two FGC tubes. The largest volume fractions of the two kinds of reinforcements were noted in the FGC_C tube sample as 13 φ/% of primary Si at the inner zone and 36.5 φ/% of primary Al_3Ni at the outer zone. As shown in **Figure 6b**, the volume fraction of primary Al_3Ni particles in the transition zones of FGCs varied from (17 to 28) φ/%, associated with primary Si particles. When FGCs were compared to the LM6 tube, the segregation of primary Si particles increased by 39.4 % in FGC_A, 51.6 % in FGC_B, and 53.9 % in FGC_C in their inner zone.

It can be summarised that two kinds of primary particles, such as primary Si and Al_3Ni, were plentiful in the inner and outer zones of the gradient composite tubes, respectively. An amount of eutectic Al_3Ni and Si existed in all the zones. Furthermore, eutectic Si flakes were found in greater quantity in the LM6 tube and decreased as the nickel concentration climbed. Because of the cooling action of the mould, very limited primary Si cuboids remained within the outer zone, whereas the fewest primary Al_3Ni particles settled in the inner zone owing to the rise in the viscosity of the melt. Primary Si and Al_3Ni particulates exhibited an evident gradient pattern along the radial direction of the FGC tubes from the inner to the outer zone. In centrifugal casting, a mould wall is a good place for beginning the solidification at a higher cooling rate, so directional solidification occurred from the wall to the mould center during the casting process. It is also believed that this situation improved the feeding

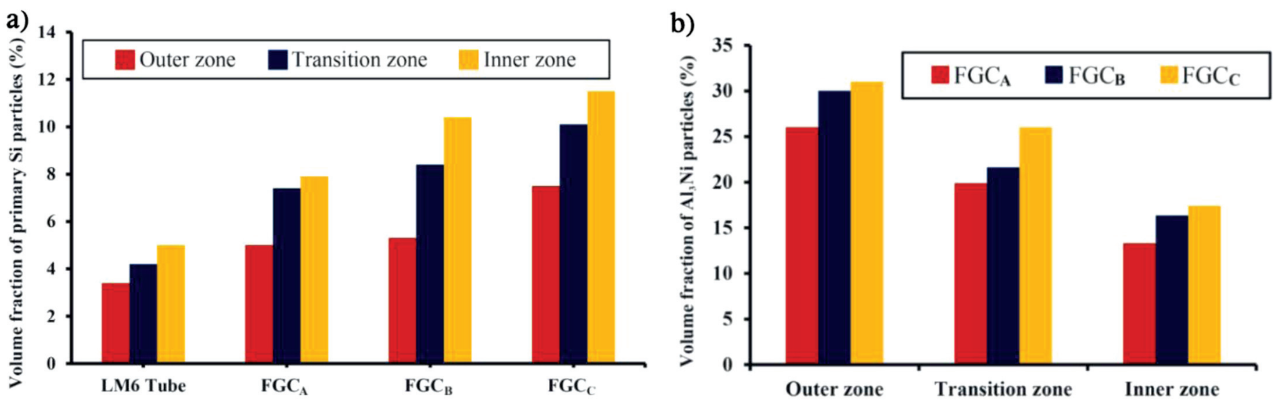

Figure 6: a) Volume fraction of primary Si particles, b) volume fraction of Al_3Ni particles at different zones of the cast tubes

potential of interdendritic regions and decreased the formation of porosity in the LM6 and FGC tubes.

3.2 Hardness

The findings from the hardness assessments of both LM6 and FGC tubes at five spots in the thickness are presented in **Figure 7**. The hardness of the FGC tubes increased compared to LM6 alloy tubes, owing mostly to precipitating hard *in-situ* Al_3Ni reinforcements (841HV). **Figure 7** shows a declining trend in hardness measured from the outside edge of the FGC tube samples. In contrast, the outer-to-inner edge hardness assessment in an LM6 tube sample revealed a distinct pattern. The peak hardness of this sample was 83 HV at its inner edge (considered as inner zone) and 76 HV at its outer edge (considered as outer zone). This minor variation between these two zones was associated with a deficit of primary Si cuboids, according to microstructural investigations of the LM6 tube. It was evident that the method in which the reinforcement phases segregate during centrifugal casting of composite melt has a direct impact on the hardness values.[29] The hardness readings for FGC tube samples followed the same trend, with hardness decreasing towards the inner edge across the radial thickness. Similar to the microstructural observations, the reported hardness values demonstrated proper gradient as a result of the segregating manner of both primary Al_3Ni blocky particles and primary Si cuboids over the radial cross-section. LM6 tube had an outside edge hardness value of 76 HV, which elevated by 15.55 %, 23.23 %, and 35.75 % in the FGC_A, FGC_B, and FGC_C, respectively. The hardness improved when intermetallic Al_3Ni precipitated in a eutectic Al-Si melt.[21] The observed increase in hardness near the outside edge of FGC tubes was mostly attributable to tri-aluminide segregation and nucleation.

The FGC_C tube sample had the highest hardness values tested from the outside edge to the inner edge, with the outer edge having the maximum hardness value of 118.30HV. This enhancement was connected to its microstructure and reinforcements segregation in such a manner that the presence of a substantial amount of *in-situ* Al_3Ni precipitates owing to the action of centrifugal force and accelerated precipitate growth rate in the composite melt. It was recognized that the rate of development of *in-situ* Al_3Ni nuclei and the temperature gradient induced were predominantly accountable for the increase in hardness in a eutectic Al-Si alloy.[30] Due to a temperature disparity (about 520 °C) between the composite melt and the GCI mould, a long time started to emerge during solidification, which promoted intermetallic Al_3Ni nucleation. Furthermore, when adding Ni in the range of (3 to 9) *w*/%, the inner edges of fabricated FGC samples having improved primary Si settlements showed hardness improvements in the order of 1.2 %, 3.5 %, and 16 % when compared to LM6 tube (inner edge = 83 HV). In comparison, it was obvious that the presented hardness values were closely related to the volume proportions of both *in-situ* Al_3Ni and primary Si precipitates (**Figures 6**).

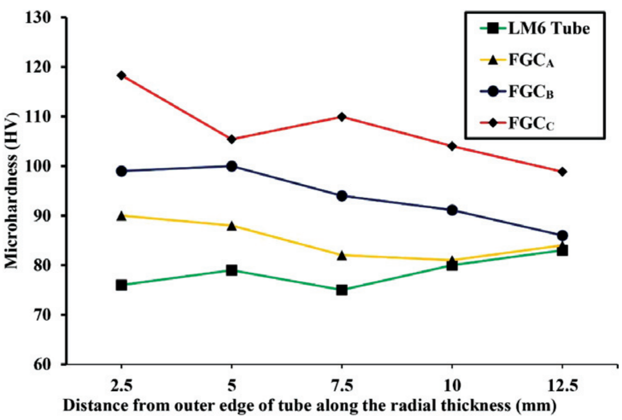

Figure 7: Variations in hardness from the outer region along the radial thickness of centrifugally cast tubes

3.3 Tensile Characteristics

The obtained tensile properties of both the LM6 tube and FGCs at three different zones are presented in **Figure 8**. All of the FGC tube specimens demonstrated higher tensile strength than the LM6 tube in all three zones. The microstructural observations suggested that the UTS improvement was due to the precipitation and strengthening influence of the Al_3Ni intermetallic phase in the FGC tubes.[10] They were wetted with the molten Al-Si alloy, resulting in good and persistent bonding between particles and matrix. This reliable interface was presumed to effectively transmit and disperse load from the matrix to the reinforcement. Generally, the tensile characteristics of the *in-situ* composites based on Al-Si alloy are dictated by microstructural features such as α-Al matrix, precipitated intermetallics, Si phase, and microporosities.[31] Owing to the existence of more primary Al_3Ni dispersoids that had greater bonding with the matrix, the outer zones of FGCs exhibited elevated tensile strength. The young's modulus and UTS of Al_3Ni tri-aluminide have been reported to be 116 GPa to 152 GPa and 2160 MPa, respectively, which are much higher than Al-Si matrix (E = 70 GPa & UTS = 37 MPa).[11] Inspite of these high properties, the load acting was transferred to the intermetallic particles, which performed as load-bearing structures to postpone the fracture during the tensile test.

As indicated in **Figure 8a**, the FGC_C tube outer zone specimen with the highest proportion of Al_3Ni (31 φ/%) had a maximum tensile strength of 203 MPa. This could possibly be viewed as a result of the action of hard Al_3Ni reinforcing particles, which impeded the plastic flow of the aluminium matrix. In contrast, the LM6 tube presented only 137 MPa in the same zone, which is 32.5 % less than FGC_C. However, the nickel-added FGCs showed a reduction in the percentage of elongation to rupture compared with the LM6 tube, as shown in **Fig-**

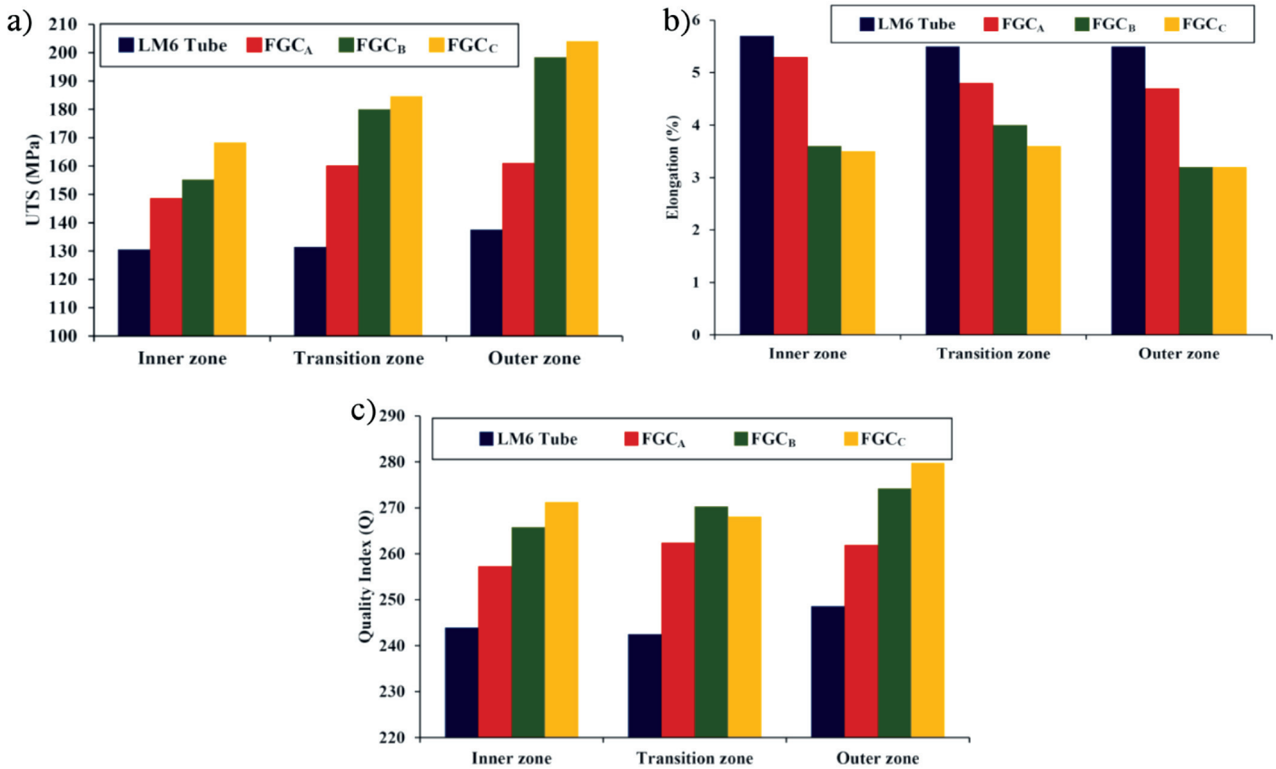

Figure 8: Tensile properties of centrifugally cast tubes in different zones: a) UTS, b) Elongation (%) and c) Quality Index (Q)

ure 8b. It was noticed that when the nickel content of the composite melt increases, the elongation decreases significantly.[10] This might be owing to the segregation of hard intermetallic Al_3Ni in the Al-Si grain boundaries. The UTS at the inner zone of the LM6 tube specimen was 130 MPa, which was greatly improved in the case of all the FGC tube specimens due to the addition of nickel. It has also been found that the fracture propensity of an Al-Si alloy increases if the microstructure consists of coarser eutectic Si flakes than cuboidal primary Si.[32] It was evident from the microstructures of the FGCs that all three zones contain eutectic phases of Si and Al_3Ni. These hard eutectic phases were believed to form an interconnected network that significantly enhanced the UTS of the FGCs by improving the load-transfer capacity.[33] As seen in microstructures (**Figure 4**), all the FGC tubes had more primary Si particles and fewer primary Al_3Ni particles in their inner zones. Furthermore, these less *in-situ* Al_3Ni intermetallics were identified as incapable to withstand much-pulling force. **Figure 8a** shows that the tensile strength increased at the inner zone from 130 MPa for the LM6 tube to 189 MPa for FGC_C. The elongation, on the other hand, reduced from 5.7 % to 2.6 %. The substantial increase in UTS at the inner zone of FGCs should be attributable to the existence of numerous primary Si particles accompanied by a few intermetallic particles, which is not the case in the LM6 tube. The LM6 tube specimen only comprised more eutectic silicon flakes with very few primary silicon particles, as shown in **Figure 4**.

The quality index (Q) has been used to evaluate the overall tensile properties of any alloy, and it is thought to be a better representation of the actual tensile property compared to either tensile strength or elongation alone.[34] It is commonly computed using Equation 6.

$$Q = \text{UTS (MPa)} + 150 \times \log(\%E) \tag{6}$$

As can be stated from **Figure 8c** that the incorporation of nickel into eutectic Al-Si alloy improves the Q greatly and hence Q values of all FGC tube specimens were greater than the LM6 tube in all three zones. When FGC tubes were chilled from the process temperature, variation in the Coefficient of thermal expansion (CTE) between the Al-Si matrix (24×10^{-6}/K) and *in-situ* Al_3Ni (14.3×10^{-6}/K) causes dislocations to occur. In addition, such dislocations are produced as a result of the existence of Al_3Ni intermetallics within the matrix, obstructing plastic deformation and contributing to the better tensile characteristics of the FGCs. As expected, the highest quality index was achieved in the FGC_C outer zone, because of the abundant presence of primary Al_3Ni precipitates and the notable presence of primary Si. The lowest Q computed for the transition zone of the LM6 tube was 242 MPa, which is 10.29 % lower than the transition zone of FGC_B. However, the presence of more *in-situ* Al_3Ni and Si phases greatly reduced the α-Al phase, lowering the ductility of the FGCs.

3.4 Tensile Fractography

The fractured surfaces of the LM6 and FGC tubes were analyzed perpendicular to the tensile axis. SEM images of The LM6 tube fractured specimens were displaying a clear brittle fracture at all three zones, as shown in **Figure 9**. However, because of the existence of primary Si particles, some ductile dimples were also observed. During the examination of the fractured surfaces, all three zones of the LM6 tube showed many cleavage facets and tear ridges. These cleavage facets were formed by the fracture of Si particles, whereas the tear ridges were created by plastic deformation and fracturing of the aluminium matrix. The glowing traces surrounding the tear ridges clearly revealed the brittle cracking of the Si particles. The inner zone of this LM6 tube is composed of comparatively more primary silicon particles, which are responsible for the decrement in tensile strength than the other two zones. Because of the stress concentration, primary Si particles were observed to crack and debond. The typical ductile dimples were also shown in the inner zone. The formation of void nuclei was reported to occur predominantly at the interfaces between the primary Si particles and the matrix, wherein stress concentrations were higher.[35]

Two kinds of explanations were attained through microstructural and fractographic evidence of LM6 tube: a) small dendrites and silicon particles showed less damage rate since they required a huge strain to attain the critical degree of disruption for causing damage and b) elongated Si phase with a long length contained coarser microstructures were more likely to crack at low loads, reducing the ductility. The presence of eutectic Si phase in all three zones across the LM6 tube caused fractures to develop quickly in the aluminium matrix, attributable to eutectic Si fragmentation. These cracks became the sources of stress, forming a network between cracks and causing an uncontrollable fracture in the specimen, as shown in **Figure 9b**.[16] The fracture mechanism associated with the LM6 tube specimens can be understood in the following ways. The imposed tensile strain caused significant plastic deformation around the Si particles in the aluminium matrix, resulting in Al-Si debonding, tear ridges, and the creation of microvoids at the interface. The microvoids linked up with each other at the Al-Si interface during tensile stress and constitute a microscopic crack. Subsequently, these microcracks became unstable, causing the ultimate failure. Also, in the eutectic, cracks at the interfaces among the aluminium matrix and Si were regularly found to develop; however, some fractured Si particles were also identified.

Figure 10 depicts the SEM fractography of the FGC_C tube at its three zones, which have the highest addition of nickel. The fractured surfaces of this specimen showed a mixed mode of ductile dimples and cleavages of brittle fracture. In particular, brittle fracture was observed in the outer zones of all three FGCs with very few dimples. The other two zones presented a mixed mode of brittle-ductile fracture. It was identified that the increase of nickel directly improved the nucleation of *in-situ* Al_3Ni phase from microstructural observation, which promoted more brittle cleavages across the radial cross-section of tubes. As can be seen in the outer zone of the FGC_C tube

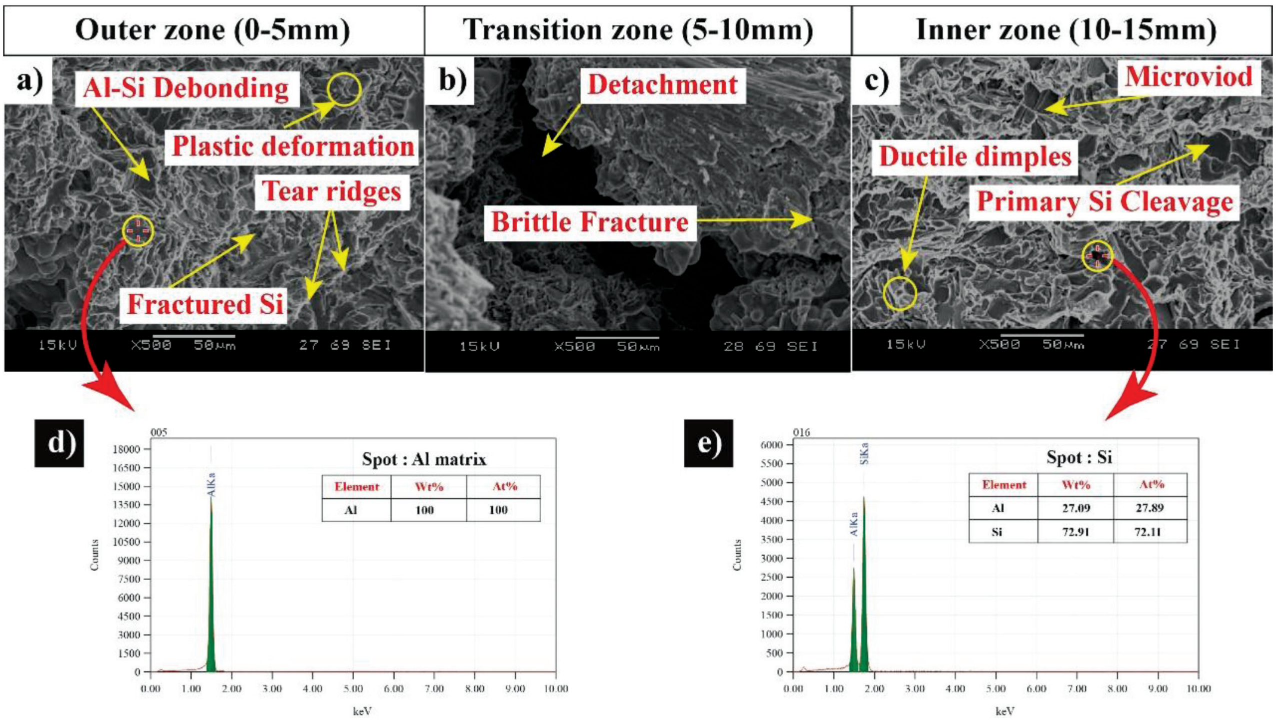

Figure 9: SEM fractographs of LM6 tube zones (a, b & c), d) EDS pattern of α-Al phase and e) Si phase

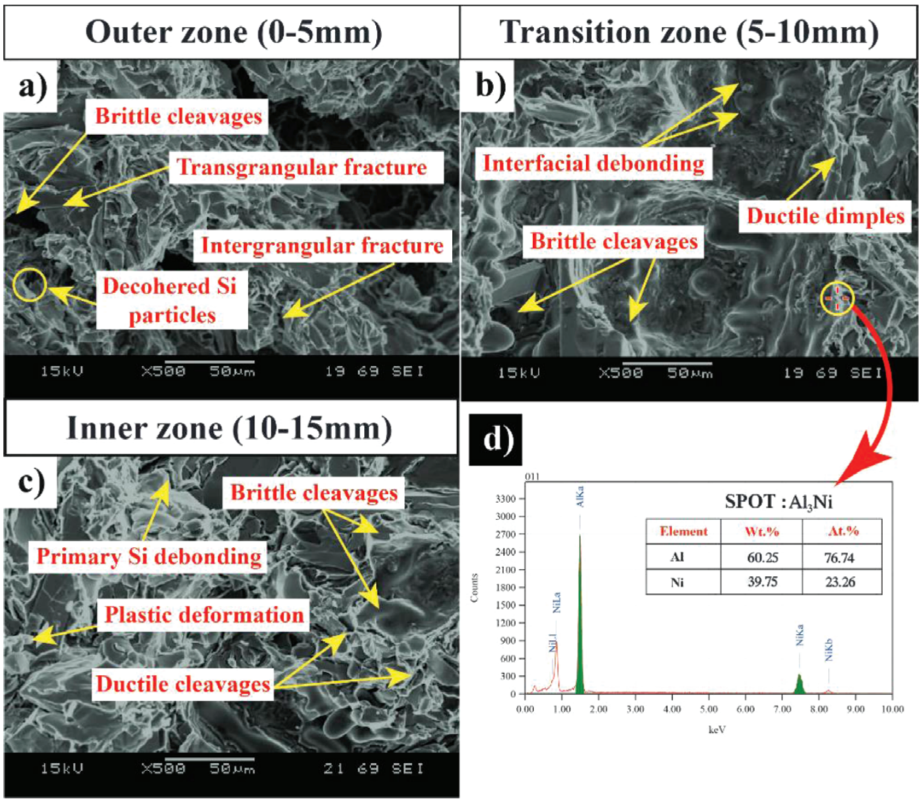

Figure 10: SEM fractographs of FGC_C tube zones (a, b & c) and EDS pattern of Al_3Ni phase (d)

specimen (**Figure 10a**), more brittle fracture arose, which presented low ductility. Fractography of FGC_C tube specimen has the following failure characteristics: i) interfacial debonding of both primary Al_3Ni and Si particles from aluminium matrix (intergranular – brittle), ii) crack propagation through Si particles (transgranular – brittle) and iii) torn out or decohered Si particles (ductile).

Debonding of the primary Si particles occurred during the first stage of tensile testing owing to plastic deformation in the α-Al matrix generated by a minor tensile force applied. The crack formed through this debonding tried to develop a severe fracture in the FGCs. However, this crack flow was restricted by the existence of *in-situ* Al_3Ni in interdendritic areas of the FGCs. This resistance to crack flow offered by the intermetallic was figured to be the key factor in the enhancement of tensile strength. With regard to the inner zones of the FGCs, more primary Si debonding failure was observed (**Figure 10c**). The scarcity of Al_3Ni tri-aluminide and availability of more α-Al matrix caused more severe crack formation and growth in the inner zones of FGCs than in the other two zones. Furthermore, because of very limited stability of the α-Al matrix, the constant tensile stress induced dislocations. These dislocations stacked up at the interface (α-Al/Si) and triggered high stress concentrations, which crushed the silicon particles and generated a crack- nucleation site.[36,37]

The presence of dimples on the fracture surfaces of FGCs can clearly identify it (**Figure 10b**). As mentioned above, these cracks were not moving through the Al_3Ni intermetallic particles, because there was no evidence of broken intermetallics on the fracture surfaces. Instead, these cracks moved along the boundaries, resulting in interfacial debonding between the Al_3Ni and the matrix.[20] According to Griffith's theory, the particle is estimated to be crushed only when the stress surpasses the Griffith threshold. The stress required to fracture a particle is expressed in Equation (7) as follows,

$$\sigma_c^p = \frac{k_c^p}{\sqrt{d}} \tag{7}$$

Where k_c^p is the fracture toughness and d is the diameter of the reinforcement particle.[38] Because no transgranular crack was observed in the Al_3Ni phase, it can be inferred that there was no superficial interface between the matrix and intermetallic. Generally, if the matrix remains smooth, the interface becomes weak and there is decoherence. EDS analysis corroborated the inclusion of *in-situ* Al_3Ni in the interdendritic vicinity, as shown in **Figure 10d**. A reinforcement particle fracture is distinctly related to its fracture toughness; hence it was evident that the FGCs included Al_3Ni intermetallics with excellent fracture toughness. The fracture initiation at the inner zone was caused by the primary Si particles and in the case of the remaining two zones, it was almost eutectic Si. In all of the FGCs, the brittle Si particles were torn out (decohered) from the α-Al matrix in these flat areas (**Figure 10a**), having left a smooth facet terrace. Despite the fracture of the brittle Si phase, these cleavage facets were more likely to form.[39] It should be recorded that the inner zone had more elongation than the outer zone. The rising concentrations of brittle Al_3Ni phase represented the decrease in the percentage of elongation to rupture from FGC_A to FGC_C, which is mainly accountable for the 3.1 % drop in elongation at all zones while attempting to compare LM6 with FGC_C tubes.

4 CONCLUSIONS

Four kinds of defect-free functionally graded composite (FGC) tubes (LM6 tube, FGC_A, FGC_B, and FGC_C) were manufactured by horizontal centrifugal casting, with nickel inclusion varying from 0 to 9 *w*/%. All three FGC tubes demonstrated more substantial gradation than the LM6 tube, which had very low gradation owing to the absence of nickel addition and the eutectic nature. The microstructures, hardness, and tensile properties of the fabricated tubes were comprehensively investigated zone by zone (inner, transition, and outer zone). This study discovered that adding nickel to the LM6 alloy generated *in-situ* Al_3Ni, which inhibited the growth of eutectic Si flakes and nucleated cuboidal primary Si.

Due to the notable segregation of primary Si cuboids in the inner zone, zone-wise characterization of the LM6 tube revealed only a marginal gradient structure across the radial thickness. Tensile fractography revealed the brittle fracture, which was induced by the abundant availability of the elongated eutectic Si phase. FGC tubes exhibited three distinct microstructural features in their radial cross-section due to the segregation of primary Si and *in-situ* Al_3Ni during solidification related to their density difference. A richly *in-situ* Al_3Ni accumulated outer zone, a more cuboidal Si-deposited inner zone and a mixed transition zone were observed and this gradient structure influenced the properties.

It was also deduced that increasing the amount of nickel in the composite melt increases the gradation, resulting in distinct property differences. In comparison to the LM6 tube, the hardness of the FGC tubes improved gradually across all three zones. However, nickel-added FGCs showed a reduction in the percentage of elongation to rupture, and fracture analysis indicated a mixed mode of ductile dimples and brittle fracture cleavages.

It appears that different qualities may be tailored in LM6 alloy-based FGC in this approach by promoting various *in-situ* reinforcements, and greater attention is to be provided in the future to examine other properties of the manufactured FGC tubes.

5 REFERENCES

[1] M. Sai Charan, A. K. Naik, N. Kota, T. Laha, S. Roy, Review on developments of bulk functionally graded composite materials, Int. Mater. Rev., 67 (**2022**) 8, 797–863, doi:10.1080/09506608.2022.2026863

[2] A. Mallick, S. G. Setti, R. K. Sahu, Centrifugally cast functionally graded materials: Fabrication and challenges for probable automotive cylinder liner application, Ceram. Int., 49 (**2022**) 6, 8649-8682, doi:10.1016/j.ceramint.2022.12.148

[3] K. K. Sriram, N. Radhika, M. Sam, S. Shrihari, Studies on adhesive wear characteristics of centrifugally cast functionally graded ceramic reinforced composite, Int. J. Automot. Mech. Eng., 17 (**2020**) 4, 8274–8282, doi:10.15282/ijame.17.4.2020.05.0625

[4] R. M. Mahamood, E. T. Akinlabi: Types of functionally graded materials and their areas of application, https://link.springer.com/chapter/10.1007/978-3-319-53756-6_2, 15.02.2017

[5] C. Samson Jerold Samuel, A. Ramesh, K. Krishnamoorthy, K. Shankar Selvaraj, P. Govindan, Investigation of the mechanical properties of a squeeze-cast LM6 aluminium alloy reinforced with a zinc-coated steel-wire mesh, Mater. Tehnol., 52 (**2018**) 2, 125–131 doi:10.17222/mit.2017.019

[6] C. Contatori, N. I. Domingues Jr, R. L. Barreto, N. B. de Lima, J. Vatavuk, A. A. C. Borges, G. F. C. Almeida, A. A. Couto, Effect of Mg and Cu on microstructure, hardness and wear on functionally graded Al–19Si alloy prepared by centrifugal casting, J. Mater. Res. Technol., 9 (**2020**) 6, 15862-15873, doi:10.1016/j.jmrt.2020.11.050

[7] S. C. Ram, K. Chattopadhyay, A. Bhushan, High Temperature Dry Sliding Reciprocating Wear Behavior of Centrifugally Cast A356-Mg_2Si In-Situ Functionally Graded Composites, Silicon, 15 (**2023**), 1063–1083, doi:10.1007/s12633-022-02060-4

[8] S. M. Aktarer, D. M. Sekban, O. Saray, T. Kucukomeroglu, Z. Y. Ma, G. Purcek, Effect of two-pass friction stir processing on the microstructure and mechanical properties of as-cast binary Al–12Si alloy, Mater. Sci. Eng. A, 636 (**2015**), 311-319, doi:10.1016/j.msea.2015.03.111

[9] M. Golmohammadi, M, Atapour, A. Ashrafi, Fabrication and wear characterization of an A413/Ni surface metal matrix composite fabricated via friction stir processing, Mater. Des., 85 (**2015**), 471–482, doi:10.1016/j.matdes.2015.06.090

[10] L. Yang, W. Li, J. Du, K. Wang, P. Tang, Effect of Si and Ni contents on the fluidity of Al-Ni-Si alloys evaluated by using thermal analysis, Thermochim. Acta, 645 (**2016**), 7–15, doi:10.1016/j.tca.2016.10.013

[11] G. Miranda, O. Carvalho, D, Soares, F. S. Silva, Properties assessment of nickel particulate-reinforced aluminum composites produced by hot pressing, J. Compos. Mater., 50 (**2016**) 4, 523–531, doi:10.1177/0021998315577148

[12] T. P. D. Rajan, B. C. Pai, Developments in processing of functionally gradient metals and metal–ceramic composites: a review, Acta Metall. Sin. (Engl. Lett.), 27 (**2014**), 825–838, doi:10.1007/s40195-014-0142-3

[13] J. J. Sobczak, L. Drenchev, Metallic functionally graded materials: a specific class of advanced composites, J. Mater. Sci. Technol., 29 (**2013**) 4, 297–316, doi:10.1016/j.jmst.2013.02.006

[14] X. Lin, C. Liu, H. Xiao, Fabrication of Al–Si–Mg functionally graded materials tube reinforced with in situ Si/Mg_2Si particles by centrifugal casting, Compos. B. Eng., 45 (**2013**) 1, 8–21, doi:10.1016/j.compositesb.2012.09.001

[15] S. C. Ram, K. Chattopadhyay, I. Chakrabarty, High temperature tensile properties of centrifugally cast in-situ Al-Mg_2Si functionally graded composites for automotive cylinder block liners, J. Alloys Compd., 724 (**2017**), 84–97, doi:10.1016/j.jallcom.2017.06.306

[16] L. I. Bo, W. A. N. G. Kai, M. X. Liu, H. S. Xue, Z. Z. Zhu, C. M. Liu, Effects of temperature on fracture behavior of Al-based in-situ composites reinforced with Mg_2Si and Si particles fabricated by centrifugal casting, Trans. Nonferrous Met. Soc. China, 23 (**2013**) 4, 923–930, doi:10.1016/S1003-6326(13)62549-2

[17] N. B. Duque, Z. H. Melgarejo, O. M. Suhrez, Functionally graded aluminum matrix composites produced by centrifugal casting, Mater. Charact., 55 (**2005**) 2, 167–171, doi:10.1016/j.matchar.2005.04.005

[18] T. P. D. Rajan, R. M. Pillai, B. C. Pai, Functionally graded Al-Al_3Ni in situ intermetallic composites: fabrication and microstructural characterization, J. Alloys Compd., 453 (**2008**) 1–2, L4–L7, doi:10.1016/j.jallcom.2006.11.181

[19] S. El-Hadad, H. Sato, Y. Watanabe, Wear of Al/Al_3Zr functionally graded materials fabricated by centrifugal solid-particle method, J. Mater. Process. Technol., 210 (**2010**) 15, 2245–2251, doi:10.1016/j.jmatprotec.2010.08.012

[20] U. Bayram, N. Maraşlı, Influence of growth rate on eutectic spacing, microhardness, and ultimate tensile strength in the directionally solidified Al-Cu-Ni eutectic alloy, Metall. Mater. Trans. B, 49(**2018**), 3293–3305, doi:10.1007/s11663-018-1404-7

[21] A. K. Gupta, B. K. Prasad, R. K. Pajnoo, S. Das, Effects of T6 heat treatment on mechanical, abrasive and erosive-corrosive wear properties of eutectic Al–Si alloy, Trans. Nonferrous Met. Soc. China, 22 (**2012**) 5, 1041–1050, doi:10.1016/S1003-6326(11)61281-8

[22] V. A. Hosseini, S. G. Shabestari, R. Gholizadeh, Study on the effect of cooling rate on the solidification parameters, microstructure, and mechanical properties of LM13 alloy using cooling curve thermal analysis technique, Mater. Des., 50 (**2013**), 7–14, doi:10.1016/j.matdes.2013.02.088

[23] R. Kakitani, C.B. Cruz, T.S. Lima, C. Brito, A. Garcia, N. Cheung, Transient directional solidification of a eutectic Al-Si-Ni alloy: Macrostructure, microstructure, dendritic growth and hardness, Mater., 7 (**2019**), 100358, doi:10.1016/j.mtla.2019.100358

[24] Y. Wang, H. Liao, Y. Wu, J. Yang, Effect of Si content on microstructure and mechanical properties of Al–Si–Mg alloys, Mater. Des., 53 (**2014**), 634–638, doi:10.1016/j.matdes.2013.07.067

[25] U. Böyük, S. Engin, N. Maraşlı, Microstructural characterization of unidirectional solidified eutectic Al–Si–Ni alloy, Mater. Charact., 62 (**2011**) 9, 844–851, doi:10.1016/j.matchar.2011.05.010

[26] S. Mudry, I. Shtablavyi, Cluster structure in Al-Si eutectic melt with solid Ni particles, Chem. Met. Alloys, 1 (**2008**), 163–167, http://www.chemetal-journal.org/ejournal2/chemetal_CMA0051.pdf

[27] Y. Watanabe, R. Sato, I. S. Kim, S. Miura, H. Miura, Functionally graded material fabricated by a centrifugal method from ZK60A magnesium alloy, Mater. Trans., 46 (**2005**) 5, 944–949, doi:10.2320/matertrans.46.944

[28] X. Lin, C. Liu, Y. Zhai, K. Wang, Influences of Si and Mg contents on microstructures of Al–xSi–yMg functionally gradient composites reinforced with in situ primary Si and Mg_2Si particles by centrifugal casting, J. Mater. Sci., 46 (**2011**), 1058–1075, doi:10.1007/s10853-010-4874-9

[29] M. M. Rahvard, M. Tamizifar, S. M. A. Boutorabi, S. G. Shiri, Characterization of the graded distribution of primary particles and wear behavior in the A390 alloy ring with various Mg contents fabricated by centrifugal casting, Mater. Des., 56 (**2014**), 105–114, doi:10.1016/j.matdes.2013.10.070

[30] U. Böyük, Physical and mechanical properties of Al-Si-Ni eutectic alloy, Met. Mater. Int., 18 (**2012**), 933–938, doi:10.1007/s12540-012-6004-5

[31] T. Lu, J. Wu, Y. Pan, S. Tao, Y. Chen, Optimizing the tensile properties of Al–11Si–0.3 Mg alloys: Role of Cu addition, J. Alloys Compd., 631 (**2015**), 276–282, doi:10.1016/j.jallcom.2015.01.107

[32] Y. C. Tzeng, S. Y. Jian, Effects of the addition of trace amounts of Sc on the microstructure and mechanical properties of Al-11.6 Si alloys, Mater. Sci. Eng. A, 723 (**2018**), 22–28, doi:10.1016/j.msea.2018.03.016

[33] F. Stadler, H. Antrekowitsch, W. Fragner, H. Kaufmann, P. J. Uggowitzer, Effect of main alloying elements on strength of Al–Si foundry alloys at elevated temperatures, Int. J. Cast Met. Res., 25 (**2012**) 4, 215–224, doi:10.1179/1743133612Y.0000000004

[34] N. Soltani, A. Bahrami, M. I. Pech-Canul, The effect of Ti on mechanical properties of extruded in-situ Al-15 pct Mg_2Si composite, Metall. Mater. Trans. A, 44 (2013), 4366–4373, doi:10.1007/s11661-013-1747-2

[35] F. Wang, B. Yang, X. J. Duan, B. Q. Xiong, J.S. Zhang, The microstructure and mechanical properties of spray-deposited hypereutectic Al–Si–Fe alloy, J. Mater. Process. Technol., 137 (**2003**) 1–3, 191–194, doi:10.1016/S0924-0136(02)01074-9

[36] E. D. Eidel'man, M.A. Durnev, Design of gradient composites of aluminum and graphite by the centrifugal-casting method, Tech. Phys., 63 (**2018**) 11, 1615–1619, doi:10.1134/S1063784218110105

[37] Y. Nemri, B. Gueddouar, M. E. A. Benamar, T. Sahraoui, N. Chiker, M. Hadji, Effect of Mg and Zn contents on the microstructures and mechanical properties of Al–Si–Cu–Mg alloys, Int. J. Met., 12 (**2018**), 20–27, doi:10.1007/s40962-017-0134-y

[38] H. Feng, J. K. Yu, W. Tan, Microstructure and thermal properties of diamond/aluminum composites with TiC coating on diamond particles, Mater. Chem. Phys., 124 (**2010**) 1, 851–855, doi:10.1016/j.matchemphys.2010.08.003

[39] G. H. Zhang, J. X. Zhang, B. C. Li, C. A. I. Wei, Characterization of tensile fracture in heavily alloyed Al-Si piston alloy, Prog. Nat. Sci.: Mater. Int., 21 (**2011**) 5, 380–385, doi:10.1016/S1002-0071(12)60073-2